Batteries & Supercaps

Research Article
doi.org/10.1002/batt.202300144

Chemistry Europe
European Chemical Societies Publishing

www.batteries-supercaps.org

VIP *Very Important Paper*

Prolonged Life Lithium Metal Batteries Enabled by Introducing Abundant Lithium Nitrate in Commercial Carbonate Electrolytes

Qiongjie Ke,[a] Qingshuai Xu,[a] Xuejun Lai,[a] Minghui Li,[a] Jianhui Li,[c] Keyou Yan,*[a, b] and Yongcai Qiu*[a, b]

Carbonate electrolytes have been extensively used as commercial electrolytes in lithium-ion batteries (LIBs) because of its high oxidative stability. However, the organic-inorganic solid electrolyte interphase (SEI) formed on the lithium (Li) metal surface is too fragile to endure huge volume fluctuation during Li plating/stripping cycles in carbonate electrolytes. Herein, a chemically stable inorganic-rich SEI was constructed on Li metal anodes by dissolving 5.5 M $LiNO_3$ in N,N-dimethylformamide (DMF) into carbonate electrolytes as an additive. The Li^+ solvation structure coordinated with NO_3^- and DMF molecules favors the formation of Li_xN_y, LiN_xO_y, and LiF in the SEI film, which have been proved to increase the interfacial energy and improve the ionic diffusion as well as the mechanical strength of the SEI. Therefore, the designed carbonate electrolyte enhances the stable cycling of Li symmetric cells up to 700 h, with a high Coulombic efficiency (CE) of 99.0% by Aurbach CE test. When paired with $LiFePO_4$ cathode, the coin cells achieve an outstanding average CE of 99.5% and 86.5% retention of initial capacity after 300 cycles.

Introduction

To meet the ever-rising demand for electric vehicles and portable electronics with long battery endurance and fast charge-discharge capability, lithium (Li) metal batteries (LMBs) have seized more attention and long-term pursuit in recent years due to its most anodic-potential (−3.04 V vs. standard hydrogen electrode) and much higher capacity (3860 mAh/g) comparing to other candidates.[1–4] However, the Li metal with strong metal activity tends to cause inevitable reactions in the commercial electrolyte and disturbs the homogeneous ions flux between electrodes, resulting in Li dendritic morphology and unstable organic-inorganic solid electrolyte interphase (SEI) film.[5–8] Moreover, the natural SEI film is mechanically inflexible and chemically delicate under electrochemical process. It cannot bear the interfacial volume fluctuations caused by Li dendrite growth upon cycling, leading to low Coulombic efficiency (CE), quick electrodes failure as well as safety issues.[9–12] Therefore, a feasible approach to regulate the SEI is highly required.

It has been proved that inorganic-rich SEI constructed by inorganic Li compounds (such as LiF, Li_2O, Li_3N, etc.) can regulate the Li deposition behavior and improve the cycling stability of LMBs.[13–15] The inorganic-rich SEI has weak bonding (lithiophobicity) with Li metal, which alleviates the same volume change as Li during cycling, which further guarantees the structural integrity of the SEI film. Meanwhile, the ceramic SEI is highly ionic conductive, mechanically flexible, and chemically inactive, it can hasten the Li ions transmission through the SEI interface, curb dendritic growth and mitigate the continuous consumption of electrolyte. Consequently, it promotes Li cycling efficiency and prevents short-circuits from separator penetrating caused by sharp dendrites.

In recent years, nitride-rich SEI film featured with high nitrogen containing Li compounds derived from the decomposition of $LiNO_3$ has been demonstrated as an effective artificial SEI for Li-S and Li-O_2 batteries.[16–19] $LiNO_3$ in ether-based electrolytes plays a crucial role as an electrolyte additive, it can be reduced to LiN_xO_y, Li_3N and other substances under electrochemical reaction. The as-formed high ion conductive film plays a critical role in Li ions transport and Li dendritic growth suppression. However, $LiNO_3$ has low solubility in commercial carbonate electrolytes (lower than 0.012 M).[20]

Adding $LiNO_3$ solubilizers in carbonate electrolytes is one of the proper methods to regulate the dissolution behavior of $LiNO_3$. Solid solubilizers such as copper fluoride, tin trifluoromethane-sulfonate and tris(pentaflurophenyl)borane have been demonstrated as efficient solubilizers in carbonate electrolytes.[21–23] However, these $LiNO_3$ solubilizer additives fail to stabilize the SEI, resulting in lower Li plating/stripping CE. Alternatively, using solvent dimethyl sulfoxide (DMSO) as a $LiNO_3$ solubilizer in fluoroethylene carbonate (FEC) electrolytes can effectively enhance the cycling performance of LMBs with

[a] Dr. Q. Ke, Dr. Q. Xu, Dr. X. Lai, Dr. M. Li, Prof. K. Yan, Prof. Y. Qiu
School of Environment and Energy, South China University of Technology, Guangzhou 510006, China
E-mail: kyyan@scut.edu.cn
ycqiu@scut.edu.cn
[b] Prof. K. Yan, Prof. Y. Qiu
State Key Laboratory of Luminescent Materials and Devices, South China University of Technology, Guangzhou, China
[c] Dr. J. Li
School of Materials and New Energy, South China Normal University, Shanwei 516600, China

Supporting information for this article is available on the WWW under https://doi.org/10.1002/batt.202300144

Research Article
doi.org/10.1002/batt.202300144
Chemistry Europe
European Chemical Societies Publishing

high CE,[24] yet the presence of large amount of FEC restricts its practical application in commercial batteries. Therefore, a facile and efficient method capable of dissolving high concentration $LiNO_3$ of LMBs is imperative.

The donor number (DN) has been considered to be feasible for predicting the interaction between inorganic salts and electrolytes.[25,26] Basically, electrolytes with high DN are capable of dissolving inorganic salts, promoting solvation process of electrophilic cations and reducing the solvation separated ions pair.[27] The solution molecules of electrolyte and inorganic salts will attach electrophilic cations to form a solvated shell structure, and the central cation is likely to attract the electrons from surrounding molecules, which further reduces the LUMO energy of surrounding molecules and leads to the preferential reduction of inorganic salts.[28,29] As for $LiNO_3$ in the electrolytes with high DN, high donocity circumstance enables NO_3^- to reduce to inorganic nitrogen compounds which contribute to the fabrication of inorganic-rich SEI film under electrochemical process.

To our best knowledge, N,N-dimethylformamide (DMF) is one of the candidates with higher DN than that of NO_3^-,[30–32] and its solubility of $LiNO_3$ is much higher (5.5 M at 25 °C) than that for carbonate electrolytes. Herein, the 1.0 M $LiPF_6$ in ethylene carbonate/ethyl methyl carbonate/diethyl carbonate (EC/EMC/DEC, 3:5:2 by weight) solution was chosen as the standard electrolyte (denoted as STD electrolyte) because it is one of the best carbonate-based electrolyte system for lithium batteries and has been used as commercial electrolyte. We introduce DMF as $LiNO_3$-solubilizer to address the dissolution obstacle of $LiNO_3$. The as-prepared electrolyte (denote as $LiNO_3$-DMF) provides a circumstance of high concentration of $LiNO_3$, which promotes a consistent formation of uniform inorganic-rich SEI film. The as-formed SEI consisting of nitrogen-containing Li compounds on the Li metal enables LMBs to provide enhanced cycling stability in symmetric cells, with 99% CE according to the Aurbach test. When paired with $LiFePO_4$ (LFP) cathode, the cell shows improved capacity retention (86.5% retention after 300 cycles of the initial capacity).

Results and Discussion

The preparation of high concentration $LiNO_3$-DMF solution and formation mechanism of the inorganic-rich SEI film are schematically illustrated in Figure 1(a). The $LiNO_3$-DMF solvation structure is constructed spontaneously, when $LiNO_3$-DMF is added into the electrolyte. As shown in Figure S1, no precipitation is observed when 4.7 wt% of 5.5 M $LiNO_3$-DMF was added to the blank electrolyte. To study the coordination interaction between $LiNO_3$ and DMF, the Raman spectra of the pure DMF and DMF with 5.5 M $LiNO_3$ were compared. As shown in Figure S2(a), the additional peaks at around 1050 cm^{-1} after dissolving $LiNO_3$ into DMF mainly ascribes to the presence of NO_3^- in the electrolyte, and most of the Raman bands shift to the higher value due to the presence of $LiNO_3$ except the CNC symmetric stretching at 866 cm^{-1} and CO stretching at 1660 cm^{-1}. The shifting can be considered as the promotion of Li^+ solvated DMF structure as well as the association of Li^+ ions with NO_3^- ions. This result is similar to that in $LiClO_4$-DMF solutions.[33] Meanwhile, the Raman spectra of carbonate electrolyte with $LiNO_3$-DMF additives exhibits two additional peaks at 1420 and 672 cm^{-1}, and the position is the same as that shifting peaks above, which further confirms the participation of NO_3^- ions in the Li^+ solvation structure.

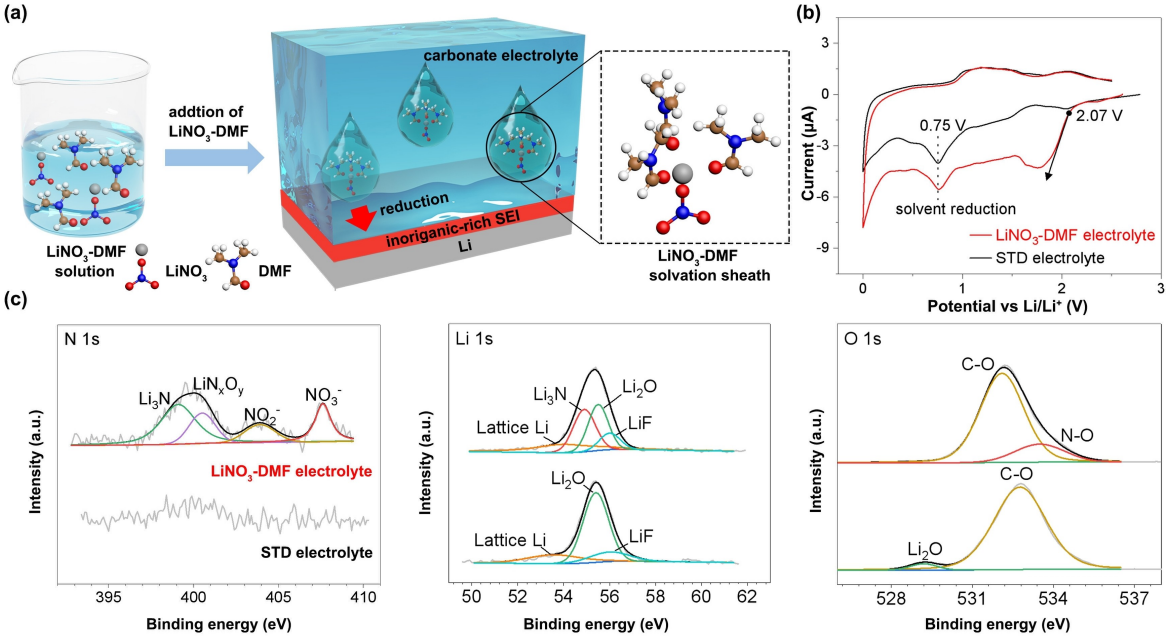

Figure 1. a) Schematics illustration of solvation sheath of Li ions and the SEI formed in $LiNO_3$-DMF electrolyte, in which PF_6^- is not shown. b) CV curves of Li||Cu half cells scanned between 0 V–2.5 V at 0.1 mV/s in different electrolyte. c) XPS spectra of N 1s, Li 1s and O 1s of the LMA surface with $LiNO_3$-DMF and STD electrolytes after 20 cycles.

Generally, both DMF molecules and NO_3^- participate in the formation of solvation sheath of Li ions in the carbonate electrolyte. Solvated Li ions connected with NO_3^- and DMF molecules forms a large solvation sheath and further promotes the preferential reduction of NO_3^-, leading to the formation of high ion-conductive substances, such as LiN_xO_y and Li_3N. It should be noted that PF_6^- can participate in the solvation sheath of Li ions as well, which contributes to the formation of LiF.[34] These inorganic ceramics associated with each other successfully fabricate an inorganic-rich SEI film with rapid Li-ion diffusion and low diffusion energy on the surface. In contrast, the solvation sheath in STD electrolyte is mainly derived from the organic compounds and the small amount of PF_6^- within the electrolyte, which cannot contribute to the formation of a robust SEI film, thus leading to uneven Li deposition and dendrite growth.

To demonstrate the preferential reduction and evaluate the reduction potential of $LiNO_3$ in $LiNO_3$-DMF electrolyte, the cyclic voltammetry (CV) test was further conducted on Li||Cu cells at a scanning rate of 0.1 mV/s in a potential range from 2.5 V to 0.0 V in aim at allowing fully decomposition of $LiNO_3$ while neglecting Li metal deposition. The Cu film was first immersed in dilute hydrochloric acid solution for 30 min follow by washing with anhydrous ethanol three times to eliminate copper oxide on Cu electrode surfaces. As shown in Figure 1(b). The cathodic peek around 0.75 V is attributed to the reduction of the carbonate solvent, which is irrelevant to $LiNO_3$ additives. Compared with the STD electrolyte, a significant reduction slope from 2.07 V to 1.5 V can be clearly seen in $LiNO_3$-DMF electrolyte, which is assigned to the reduction of $LiNO_3$. Meanwhile, this reduction peak exhibits a stronger intensity than STD-$LiNO_3$ electrolyte, and an obvious position shift can be observed as well (Figure S3), demonstrating that the solvation structure of $LiNO_3$-DMF significantly leads to the preferential reduction of $LiNO_3$ in the first charging/discharging cycle.

To verify the SEI compositions of $LiNO_3$-DMF electrolyte, the X-ray photoelectron spectroscopy (XPS) was further characterized on the Li anodes after 20 plating/stripping cycles (1 mA/cm^2, 1 mAh/cm^2) in $LiNO_3$-DMF and STD electrolytes. The cycled anodes were transferred under an inert Ar atmosphere to neglect the contamination by air or moisture. As shown in Figure 1c and Figure S4. The N 1s spectrum of the routine SEI film formed in the STD electrolyte exhibits no obvious signal of N, indicating the absence of nitrogen compounds. In sharp contrast, the SEI film formed in $LiNO_3$-DMF exhibits four peaks in the N 1s spectrum at 399.1, 400.5, 403.9 and 407.6 eV corresponding to Li_xN_y, Li_xNO_y, NO_2^- and NO_3^-, respectively. Moreover, the additional LiN_3 content from the Li 1s spectrum at 54.9 eV and N–O bond from the O 1s spectrum at 533.5 eV of $LiNO_3$-DMF electrolyte further reveals that the more inorganic nitrogen containing grains derived from the decomposition of $LiNO_3$ formed in the resulting SEI. As we discussed above, those nitrogen containing ceramics participates together can form an inert SEI film close to Li metal, which effectively boosts the ionic diffusivity, regulates the nucleation of Li as well as suppresses Li dendrites due to its high ionic conductivity, low chemical activity and high mechanical strength. Thus, the rapid and uniform deposition of Li ions and stable cycling can be achieved.[35,36] In the case of the F 1s spectrum, the specific LiF and Li_xPF_y signals are observed in both electrolytes at 685.2 and 685.9 eV respectively, which results from the decomposition of $LiPF_6$ salt. For the C 1s spectrum, the C–C/C–H (around 284.7 eV), C–O (286.2 eV) and C=C/–CO_3^-– (around 289.5 eV) peaks can be observed in both electrolytes, representing that the organic components derived from carbonate solvents exist in both SEI film. Therefore, there is an abundance of LiF, Li_xN_y and LiN_xO_y in the resulting SEI film, enabling dendrite-free Li deposition and enhanced battery performance.

The long-term cycling performances of LMBs in various electrolytes is studied to evaluate the interfacial stability of Li metal anodes via corresponding symmetrical cells at a fixed current density of 1 mA/cm^2. To optimize the additive composition, $LiNO_3$-DMF additives with different $LiNO_3$ concentrations were first separately added into blank electrolytes at a fixed amount (4.7 wt% of additive). As shown in Figure S5, the lifespan of symmetric cells significantly increases from 250 to 700 h, when the $LiNO_3$ salt concentration in $LiNO_3$-DMF increases from 2 to 5.5 M (saturated state). As shown in Figures 2(a and b) and S6. The cell with STD electrolyte exhibits poor cycling stability and large voltage polarization after 160 h, indicating rapid destruction of SEI film and electrolyte consumption. Despite the cycling stability of the cell with STD-$LiNO_3$ electrolyte is improved owing to the introduction of $LiNO_3$, however it still fails after 300 h. Moreover, the cell with only DMF as electrolyte additive shows the worst cycling performance than STD electrolyte.

In sharp contrast, the cell with $LiNO_3$-DMF electrolyte can cycle for more than 700 h with a low overpotential below 50 mV and exhibit no sign of short circuit. Apparently, high solubility of $LiNO_3$ indeed enables a more stable interphase in LMA. Figures 2(c and d) and S7 display the electrode morphology of Li anode surface in STD, $LiNO_3$-DMF and STD-$LiNO_3$ electrolytes after 100 cycles. The bare Li anode already reveals a distinct dendritic morphology and dead Li on its surface, which is consistent with the rapid cell failure. Meanwhile, Li anode with STD-$LiNO_3$ electrolyte displays a notably rough and porous surface, but Li dendrites can still be evidenced on it. In sharp contrast, the cycled Li anode in $LiNO_3$-DMF electrolyte remains a packed and smooth surface (Figure 2d).

By conducting electrochemical impedance testing on stainless steel symmetric cells assembled with each electrolyte, the ion conductivity was evaluated, and the effect of the $LiNO_3$-DMF solvation structure on ion conductivity was explored. The testing results are shown in Figure 2(e), the $LiNO_3$-DMF electrolyte exhibits promoted ion conductivity of 5.85×10^{-4} S/cm, compared with that of STD-$LiNO_3$ electrolyte (5.22×10^{-4} S/cm) and STD electrolyte (3.86×10^{-4} S/cm), the reason mainly ascribes to the improving dissolution capacity of $LiNO_3$ due to the introduction of $LiNO_3$-DMF solvation structure, further increasing the Li^+ ions transport capability of $LiNO_3$-DMF electrolyte.

Research Article
doi.org/10.1002/batt.202300144
Chemistry Europe
European Chemical Societies Publishing

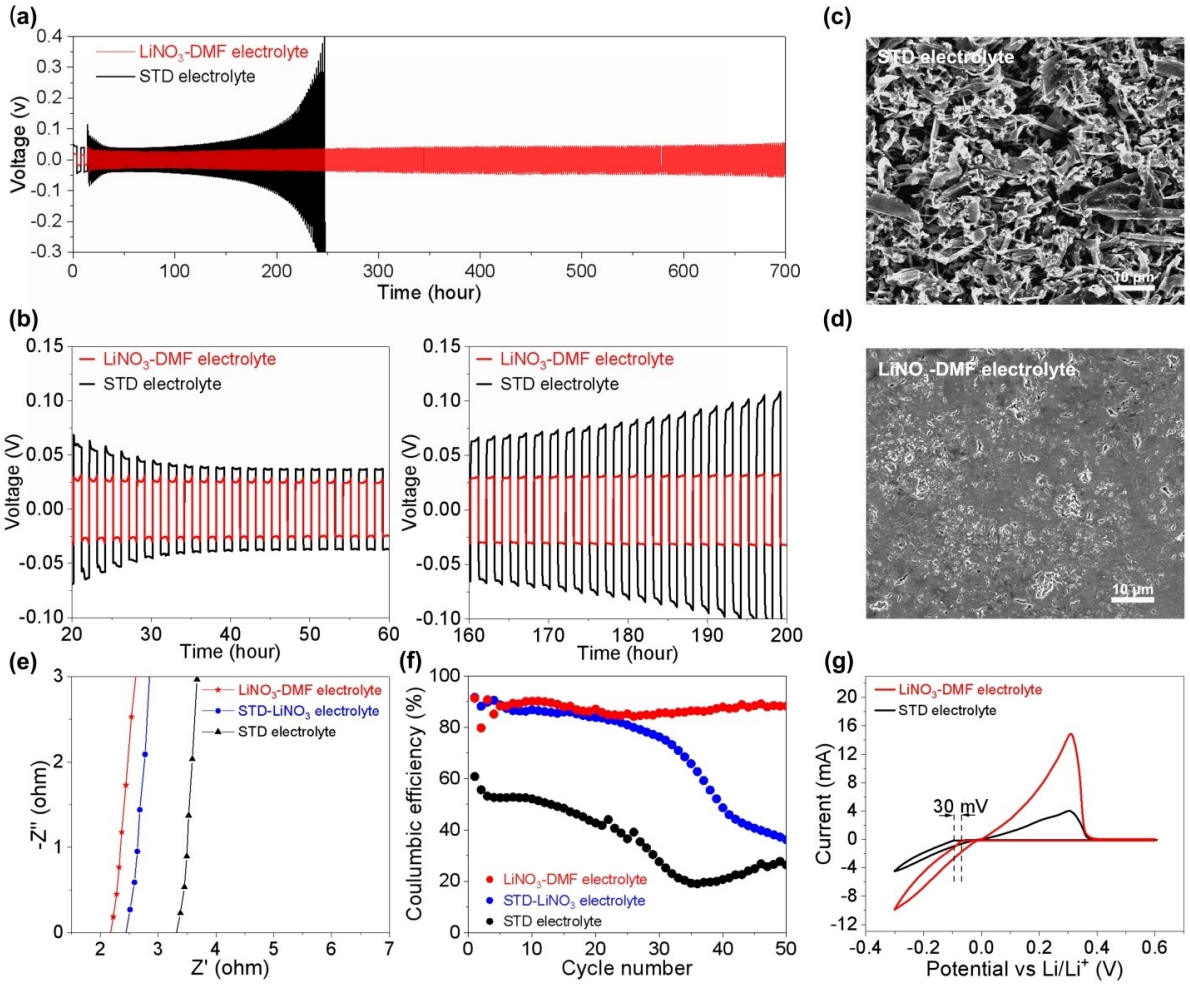

Figure 2. a) Voltage profiles of Li||Li symmetric cells at a current density of 1.0 mA/cm^2 with a plating/stripping capacity of 1 mAh/cm^2, and b) corresponding enlarged view of voltage profiles at different cycles. Surface SEM images of LMA with c) STD and d) $LiNO_3$-DMF electrolytes after 100 cycles at a current density of 1 mA/cm^2 with a plating/stripping capacity of 1 mAh/cm^2. e) Ion conductivity and f) Coulombic efficiencies (CE) in different electrolytes. g) CV curves for Li plating/stripping between −0.3 V–0.6 V at a scan rate of 2 mV/s.

Generally, dendrites formation and dead Li appearance signify the increase of Li^+ transport barriers and cell resistance, which was confirmed by electrochemical impedance spectroscopy (EIS) measurements. The interfacial resistances obtained by fitting are shown in Figure S8. The bare Li anodes for pristine cells show interfacial resistance of 68.2 and 102.8 Ω in $LiNO_3$-DMF and STD electrolyte, respectively. The smaller resistance of pristine cell with $LiNO_3$-DMF can be assigned to the initial dissolution of $LiNO_3$ in electrolyte, which acts as the pathway for Li^+ ions transport. Subsequently, after 50 cycles, the R_s of Li anode in $LiNO_3$-DMF electrolyte shows a significant decrease to 21.3 Ω and remains the same level after 100 cycles (22.8 Ω). In contrast to the cell with $LiNO_3$-DMF electrolyte, the Rs of anode in STD electrolyte experiences a reduction to 23.2 Ω after 50 cycles firstly and a large increase to 166.4 Ω after 100 cycles, subsequently, which displays rather 6 times higher resistance than that of the $LiNO_3$-DMF cell after long-term cycling because of the low ionic conductivity of the cracking SEI film.

The Coulombic efficiency (CE) of Li plating/stripping was significantly enhanced in $LiNO_3$-DMF electrolyte. Here, the Li||Cu cells were assembled with various electrolytes to test the long-term stability of lithium metal anodes at a current density of 0.5 mA/cm^2 and deposition capacity of 1 mAh/cm^2. As shown in Figure 2(f), Li||Cu cell with STD electrolyte exhibits a lowest initial Coulombic efficiency (around 60%) and begin to decline after 10 cycles, with an average Coulombic efficiency of only 38.0% within 50 cycles, indicating that there is a serious side reaction between STD electrolyte and lithium metal. The addition of $LiNO_3$ into electrolyte improves the Coulombic efficiency of Li||Cu cell to 91.6% initially but still shows significant downward trend after 30 cycles. In sharp contrast, The Li||Cu cell containing $LiNO_3$-DMF electrolyte can stably cycle for more than 100 cycles, with an average Coulombic efficiency of 88.9% within 50 cycles, indicating that the SEI formed in $LiNO_3$-DMF electrolyte has superior stability, which effectively suppressing the side reactions between lithium metal and electrolyte, thereby improving the Coulombic efficiency and cycling lifespan of the lithium battery.

Research Article
doi.org/10.1002/batt.202300144
Chemistry Europe
European Chemical Societies Publishing

Meanwhile, Aurbach test was used to obtain an accurate determination of CE in various electrolytes.[37] As shown in Figure S9, the average CE of the cell with STD electrolyte is only 66.2%. Despite the CE of the cell with STD-$LiNO_3$ electrolyte was improved to 80.5%, it still fails to meet the demand of high-efficiency rechargeable batteries due to the low solubility of $LiNO_3$ in carbonate electrolytes. Meanwhile, the cell with $LiNO_3$-DMF electrolyte achieves a highest CE of 99.0%, suggesting that the introduction of DMF greatly promotes the solubility of $LiNO_3$, which leads to the formation of rapid Li ions diffusion pathways through SEI film. The results confirm that the $LiNO_3$-DMF as an introduced solvation structure to electrolyte guarantees high Li cycling efficiency with small voltage hysteresis.

The reaction kinetics of Li plating/stripping was examined as well by using CV test in the potential range of −0.3 V–0.6 V of Li||Cu cells. As shown in Figure 2(g), the current response of initial Li plating/stripping is significantly enhanced in $LiNO_3$-DMF electrolyte, corresponding to lower Li^+ transfer barriers through SEI and fast reaction kinetics. Signifying that the contribution of interfacial film derived from $LiNO_3$ decomposition significantly improves the electrochemical kinetics of Li deposition/dissolution.

To explore the capability endurance of LMBs, the rate performance of Li||Li symmetrical cells with $LiNO_3$-DMF and STD electrolytes were conducted under a fixed capacity of 1 mAh/cm^2 and variable current densities (0.5 to 5 mA/cm^2). As shown in Figure 3(a), the overpotential of Li plating/stripping in $LiNO_3$-DMF electrolyte presents a less increase than that of STD electrolyte with increasing current density. Specifically, irregular overpotential fluctuations with larger polarization could be seen in STD electrolyte (Figure 3b). In contrast, a much gentler voltage plateau (Figure 3c) with smaller polarization of 34, 57, 125 and 210 mV at 0.5, 1.0, 3.0 and 5.0 mA/cm^2 were observed in $LiNO_3$-DMF electrolyte. The distinction of the average overpotential between these two electrolytes can be visualized more precisely in Figure 3(d). Such enhancement indicates a more stable SEI with less impedance is achieved, which agrees well with EIS results. Furthermore, the voltage profile of Li||Li symmetrical cells in each electrolyte under a fixed current

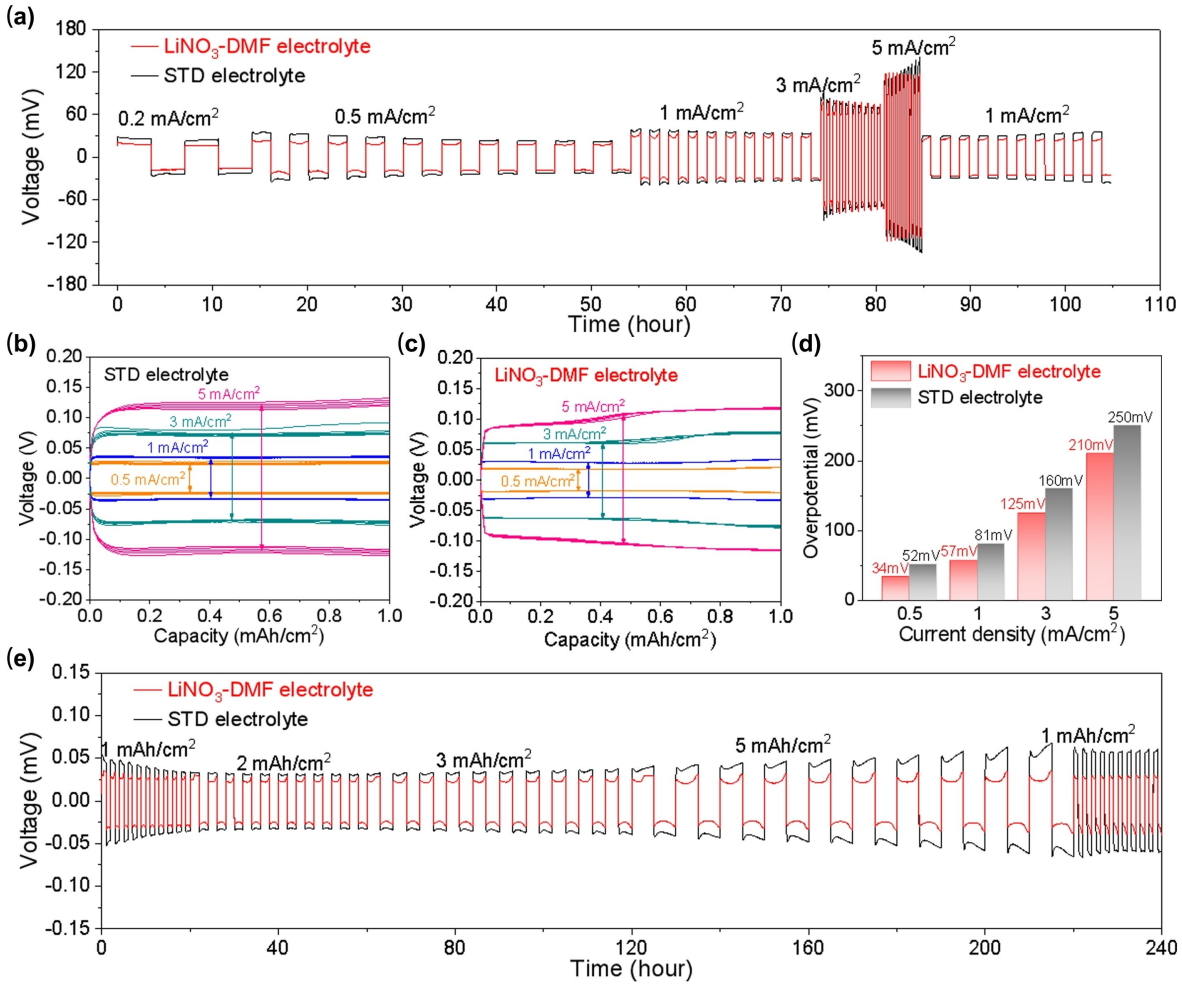

Figure 3. Symmetric cell cycling performance for different electrolytes. a) Voltage profiles of Li||Li symmetric cells under different current densities from 1 to 5 mA/cm^2 with a fixed plating/stripping capacity of 1 mAh/cm^2. Polarization profiles for Li plating/stripping in b) STD and c) $LiNO_3$-DMF electrolytes and d) detailed comparison at different current densities. e) Voltage profiles of Li||Li symmetric cells under different areal capacity from 1 to 5 mAh/cm^2 with a fixed current density of 1 mA/cm^2.

Research Article
doi.org/10.1002/batt.202300144
Chemistry Europe
European Chemical Societies Publishing

density of 1 mA/cm^2 and variable areal capacity (1 to 5 mAh/cm^2) was shown in Figure 3(e), continuous flat charging/discharging plateaus can be observed under various areal capacity for $LiNO_3$-DMF based cells, suggesting its capability of working under various areal capacity.

The deposition morphology of Li metal in the electrolyte was compared by assembling Li||Cu cells at a controlled areal capacity from 1 to 3 mAh/cm^2 with a fixed current density of 0.2 mA/cm^2. Figure 4(a–f) reveals the vivid evolution of the surface sectional images for Li morphology in STD and $LiNO_3$-DMF electrolytes with increasing areal capacity, respectively. The deposited Li in STD electrolyte seems to be porous and loose with smaller particles which are separated with each other, forming a loosely packed structure. As the deposition capacity increases, inhomogeneous and stick-like Li could be found on the top of the plated Li in the STD electrolyte, indicating uneven Li deposition. In sharp contrast, the plated Li in the $LiNO_3$-DMF electrolyte appears to have rounded edges and concatenate with each other tightly, forming a densely packaged film with less porosity. Since the introduction of $LiNO_3$ greatly reduce the side reactions between the deposited Li and $LiNO_3$-DMF electrolyte, the deposited Li remains bulk integrity with chunky structure and less tortuosity during continuous cycling, and thus resulting in high CE and low impedance.[38]

The Li||LFP full cells with $LiNO_3$-DMF and STD electrolytes were assembled and compared for investigating the electrochemical performance of $LiNO_3$-DMF electrolyte applied in practical battery. The discharge capacities and CE of LFP cells with $LiNO_3$-DMF and STD electrolytes at 1 C rate (1 C = 170 mAh/g) are displayed in Figure 5(a). The initial specific capacities of these electrolytes are at the same level (about 142 mAh/g). However, the cell with $LiNO_3$-DMF electrolyte presents a stable cycling performance over 300 cycles with capacity retention of 86.5% and a higher average CE of 99.5%. In contrast, the cell with STD electrolyte only keeps stable cycling within the ever-beginning cycles and exhibits a distinct capacity decline after 100th cycle. Moreover, Figure S10 displays the voltage profile of full cells with different electrolytes in 50th and 100th cycle. Compared to the STD electrolyte, $LiNO_3$-DMF electrolyte presents a lower voltage hysteresis of 100 mV at the 50th cycle and sustains unchanged at 100th cycle, while STD electrolyte exhibits an increasing voltage hysteresis from 140 to 210 mV. Besides, the Nyquist plots of the cells shown in Figure 5(b and c) further demonstrate that the cell with $LiNO_3$-DMF electrolyte shows a rather smaller total impedance than the blank one as well at the beginning of the SEI construction phase or after 100 and 200 cycles, indicating fast Li^+ ion transportation and low Li barrier through the interface owing to the introduction of the inorganic-rich SEI. Nevertheless, the cell with $LiNO_3$-DMF electrolyte exhibits excellent rate capability and low voltage hysteresis especially at high charging/discharging rate (Figure 5d and e), which opens up a feasible avenue for practical applications of $LiNO_3$-DMF electrolyte in Li metal batteries.

Finally, the Li||NCM811 full battery was assembled to explore the performance advantages of $LiNO_3$-DMF electrolyte in high-voltage lithium metal batteries at a rate of 1 C. Figure S11 shows the cycling performance of Li||NCM811 full cells in different electrolytes. The capacity of Li||NCM811 assembled with STD electrolyte decreased sharply after 60th cycle and failure at 90th cycle due to the oxidation decomposition of STD electrolyte at high voltage. The side reactions between lithium metal and electrolyte led to capacity decline. In contrast, Li||NCM811 cell can stably cycle over 100 cycles in $LiNO_3$-DMF electrolyte, with a capacity retention rate of 84.7% and an average Coulombic efficiency of 99.3%, indicating that $LiNO_3$-DMF electrolyte has higher compatibility with high-voltage lithium metal batteries.

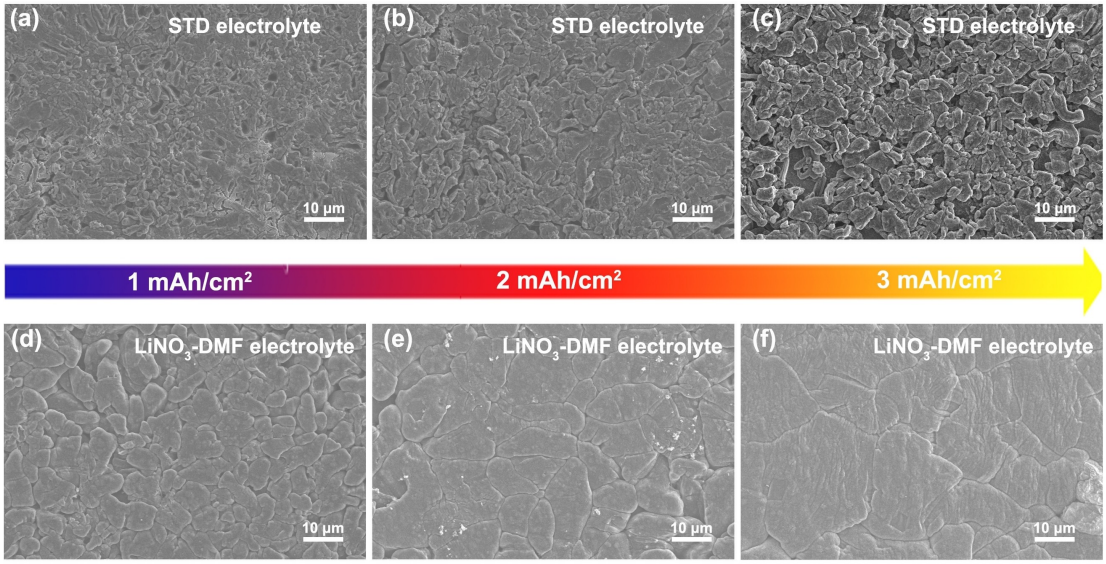

Figure 4. SEM images of the Li deposition morphology on a Cu substrate after deposition of 1, 2 and 3 mAh/cm^2 at 0.2 mA/cm^2 in a–c) STD electrolyte and d–f) $LiNO_3$-DMF electrolyte.

Research Article
doi.org/10.1002/batt.202300144
Chemistry Europe
European Chemical Societies Publishing

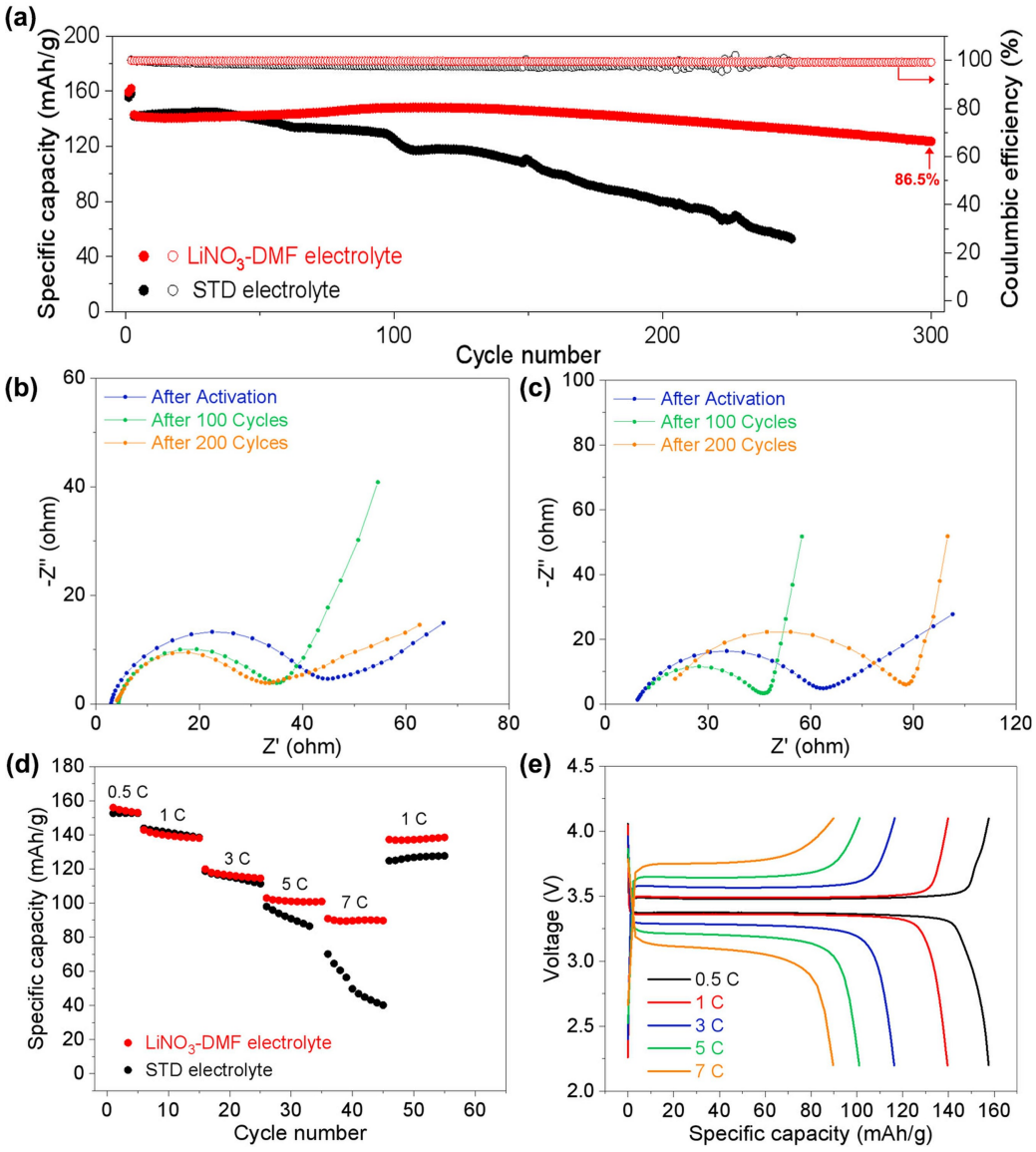

Figure 5. Electrochemical performance of Li||LFP full cells. a) Cycling performance of Li||LFP full cells at 1 C paired with LFP loading of 6 mg/cm^2. The electrochemical impedance spectra of cells with b) $LiNO_3$-DMF and c) STD electrolytes at a current density of 1 mA/cm^2 with a plating/stripping capacity of 1 mAh/cm^2. d) Rate capability of the LFP cells at various C-rates from 0.5 C to 7 C. e) Characteristic charge/discharge voltage profile of cells with $LiNO_3$-DMF electrolyte at different current densities.

Conclusions

In summary, an inorganic-rich SEI was constructed on Li metal anodes by introducing abundant $LiNO_3$ into carbonate electrolytes. The Li^+ solvation structure coordinated with NO_3^- and DMF molecules favored the formation of abundant Li_xN_y, LiN_xO_y, and LiF, which increase the interfacial energy and improve the ionic diffusion as well as the mechanical strength of the SEI. The lithiophobic inorganic-rich SEI can effectively suppress irregular Li deposition and enable dendrite-free as demonstrated by the experimental results. Consequently, we enhanced the stable cycling of Li symmetric cells up to 700 h, and a high CE of 99.0% according to the Aurbach test, which is one of the highest values ever reported for carbonate electrolytes. When paired with $LiFePO_4$ cathode, the coin cells achieved an outstanding average CE of 99.5% and capacity retention of 86.5% over 300 cycles at a practical areal loading of 6 mg/cm^2. When paired with NCM811 cathode, the coin cells maintain a capacity retention of 84.7% over 100 cycles at an areal loading of 8 mg/cm^2. This strategy reported here enables an outstanding CE as well as the stable cycling for LMBs by a facile synthetic method of electrolyte additive, which corroborates the feasibility of introducing $LiNO_3$ into carbonate electrolytes and provides a guideline for the practical application of commercial LMBs.

Experimental Section

Materials

A commercial electrolyte 1.0 M $LiPF_6$ in the EC/EMC/DEC (3:5:2 by weight) was purchased (Guangzhou Tinci Materials Technology Co., Ltd, China) and evaluated as the standard base electrolyte (denote as STD electrolyte). The $LiFePO_4$ (LFP) cathode (with the areal loading of 6 mg/cm^2) was prepared by mixing LFP (Hunan Shanshan Advanced Materials Co., Ltd, China), conductive acetylene black and polyvinylidene fluoride (PVDF) (8:1:1 by weight) with N-Methyl pyrrolidone (NMP) to form a slurry, followed by casting the slurry on aluminum foil. In an argon-filled glovebox, solvent DMF (Aladdin, 99.8%, anhydrous) was first used as the solubilizer to disperse 5.5 M $LiNO_3$ (Aladdin, 99.99%, metal basis) to form a solvent additive after stirring for 12 h at 600 rpm. The high donocity circumstance was well established and the viscosity of as-prepared solution was increased after the stirring. Therefore, to minimize the weakness caused by excessive viscosity, we added small amount of 4.7 wt% solvent additive into the STD electrolyte to form the resulting electrolyte ($LiNO_3$-DMF electrolyte). In addition, STD electrolyte with DMF (denote as STD-DMF electrolyte) and saturated $LiNO_3$ (denote as STD-$LiNO_3$ electrolyte) were used as the control electrolytes for further comparison.

Materials characterization

The composition of SEI film was detected by X-ray photoelectron spectroscopy (XPS, ESCALAB 250, USA) and the scanning electron microscope (SEM, JSM-650, Germany) was performed to monitor the morphology and microstructure of the working electrodes. The DXR2xi Raman imaging microscope (Thermo Fisher, USA) with a 532 nm diode-pumped solid-state laser was used for Raman measurements.

Electrochemical measurement

All electrochemical tests of batteries were assembled with coin-type cells (2025), 40 μL of adding electrolyte, and Celgard 2325 as separator. The asymmetric Li/$LiFePO_4$ batteries were cycled at 1 C rate between 2.2 and 4.1 V (vs. Li/Li^+). The cycling performance of all cells was conducted at Neware battery tester. Electrochemical impedance spectroscopy (EIS) was measured by PGSTAT-30 electrochemical station (Met Rohm, Netherlands). Impedance measurements on symmetric cells with stainless steel as the working electrode and counter electrode were conducted to investigate the ion conductivity, which is calculated by the equation described below:

$$\sigma = L/(A \times R)$$

where L is the distance between two stainless steel electrodes, A is the area of the electrode and R is the resistance.

The frequency range and potential amplitude in PGSTAT-30 electrochemical station were set on 10^5–0.1 Hz and 5 mV, respectively. The Aurbach CE test was used to obtain an accurate determination of CE in various electrolytes, a standard protocol was followed: (1) perform one initial formation cycle with Li deposition of 5 mAh/cm^2 on Cu foil under 0.5 mA/cm^2 current density and then (2) stripping to 1 V; (3) deposit 5 mAh/cm^2 Li on Cu foil under 0.5 mA/cm^2 as a Li reservoir; (4) repeatedly strip/deposit Li of 1 mAh/cm^2 under 0.5 mA/cm^2 for 10 cycles; (4) strip all Li to 1 V.

Acknowledgements

This work is supported by the National Key Research and Development Program of China (No. 2018YFA0209600); Science and Technology Key Project of Guangdong Province, China (No. 2020B010188002); Guangdong Innovative and Entrepreneurial Research Team Program (No. 2019ZT08 L075); Foshan Innovative and Entrepreneurial Research Team Program (No. 2018IT100031); Guangdong Pearl River Talent Program (No. 2019QN01L054); National Natural Science Foundation of China (No. 22176063) and the Fundamental Research Funds for the Central Universities (No. 2020ZYGXZR061).

Conflict of Interests

The authors declare that they have no known competing financial interests or personal relationships that could have appeared to influence the work reported in this paper.

Data Availability Statement

The authors confirm that the data supporting the findings of this study are available within the article [and/or its supplementary materials

Keywords: lithium metal batteries · $LiNO_3$ additive · solvation structure · inorganic-rich SEI

[1] S. Chu, A. Majumdar, *Nature* **2012**, *488*, 294–303.
[2] M. Armand, J.-M. Tarascon, *Nature* **2008**, *451*, 652–657.
[3] P. Albertus, S. Babinec, S. Litzelman, A. Newman, *Nat. Energy* **2018**, *3*, 16–21.
[4] X. Shen, H. Liu, X.-B. Cheng, C. Yan, J.-Q. Huang, *Energy Storage Mater.* **2018**, *12*, 161–175.
[5] X.-B. Cheng, R. Zhang, C.-Z Zhao, Q. Zhang, *Chem. Rev.* **2017**, *117*, 10403–10473.
[6] K. Xu, *Chem. Rev.* **2014**, *114*, 11503–11618.
[7] E. PELED, *J. Electrochem. Soc.* **1979**, *126*, 2047–2051.
[8] J.-C. Zheng, J.-F. Yin, D.-H. Zhang, *Sci. Adv.* **2020**, *6*, eabb1122.
[9] Y. Gao, Z.-F. Yan, J.-L. Gray, *Nat. Mater.* **2019**, *18*, 384.
[10] X. Shen, R. Zhang, X. Chen, *Adv. Energy Mater.* **2020**, *10*, 1903645.
[11] J. Liu, Z.-N. Bao, Y. Cui, *Nat. Energy* **2019**, *4*, 180–186.
[12] R. Zhang, N.-W. Li, X.-B. Cheng, *Adv. Sci.* **2017**, *4*, 201600445.
[13] W.-Y. Li, H.-B. Yao, K. Yan, *Nat. Commun.* **2015**, *6*, ncomms8436.
[14] V. Giordani, D. Tozier, J. Uddin, *Nat. Chem.* **2019**, *11*, 1133–1138.
[15] S.-F. Liu, X. Ji, J. Yue, *J. Am. Chem. Soc.* **2020**, *142*, 2438–2447.
[16] R. Elazari, G. Salitra, G. Gershinsky, *Electrochem. Commun.* **2012**, *14*, 21–24.
[17] V. Giordani, W. Walker, V.-S. Bryantsev, *J. Electrochem. Soc.* **2013**, *160*, A1544-A1550.
[18] J. Guo, Z.-Y. Wen, M.-F. Wu, J. Jin, Y. Liu, *Electrochem. Commun.* **2015**, *51*, 59–63.
[19] S.-S. Zhang, *Electrochim. Acta* **2012**, *70*, 344–348.
[20] Q.-W. Shi, Y.-R. Zhong, M. Wu, H.-Z. Wang, H.-L. Wang, *P. Natl. Acad. Sci. USA.* **2018**, *115*, 5676–5680.
[21] C. Yan, Y.-X. Yao, X. Chen, *Angew. Chem. Int. Ed.* **2018**, *57*, 14055–14059.
[22] W.-D. Zhang, Q. Wu, J.-X. Huang, *Adv. Mater.* **2020**, *32*, 2001740.
[23] S.-Y. Li, W.-D. Zhang, Q. Wu, *Angew. Chem. Int. Ed.* **2020**, *59*, 14935–14941.
[24] S.-F. Liu, X. Ji, N. Piao, *Angew. Chem. Int. Ed.* **2021**, *60*, 3661–3671.
[25] M. Baek, H. Shin, K. Char, J.-W. Choi, *Adv. Mater.* **2020**, *32*, 202005022.
[26] H. Chu, H. Noh, Y.-J. Kim, *Nat. Commun.* **2019**, *10*, s41467-018-07975-4.

[27] H.-L. Pan, X.-L. Wei, W.-A. Henderson, *Adv. Energy Mater.* **2015**, *5*, 1500113.
[28] X. Chen, Q. Zhang, *Acc. Chem. Res.* **2020**, *53*, 1992–2002.
[29] X. Chen, N. Yao, B.-S. Zeng, Q. Zhang, *Fundamental Res.* **2021**, *1*, 393–398.
[30] A. Gupta, A. Bhargav, A. Manthiram, *Adv. Energy Mater.* **2019**, *9*, 1803096.
[31] X.-W. Yu, A. Manthiram, *Phys. Chem. Chem. Phys.* **2015**, *17*, 2127–2136.
[32] P. Leghie, J.-P. Lelieur, E. Levillain, *Electrochem. Commun.* **2002**, *4*, 406–411.
[33] Z.-W. Wang, B.-Y. Huang, S.-M. Wang, *J. Electrochem. Soc.* **1997**, *144*, 778–786.
[34] X.-Q. Zhang, X. Chen, X.-B. Cheng, *Angew. Chem. Int. Ed.* **2018**, *57*, 5301–5305.
[35] C. Monroe, J. Newman, *J. Electrochem. Soc.* **2005**. *152*, A396-A404.
[36] D. Aurbach, E. Pollak, R. Elazari, *J. Electrochem. Soc.* **2009**, *156*, A694-A702.
[37] B.-D. Adams, J.-M. Zheng, X.-D. Ren, W. Xu, J.-G. Zhang, *Adv. Energy Mater.* **2018**, *8*, 1702097.
[38] S.-R. Chen, J.-M. Zheng, D.-H. Mei, *Adv. Mater.* **2018**, *30*, 1706102.

Manuscript received: April 4, 2023
Revised manuscript received: May 29, 2023
Accepted manuscript online: June 5, 2023
Version of record online: June 18, 2023